npj | clean water

Article

Published in partnership with King Fahd University of Petroleum & Minerals

https://doi.org/10.1038/s41545-024-00322-9

Effect of solution ions on the charge and performance of nanofiltration membranes

Rebecca S. Roth[1,3], Liat Birnhack[1,3], Mor Avidar[1], Elizabeth A. Hjelvik[2], Anthony P. Straub[2] & Razi Epsztein[1] ✉

Considering growing efforts to understand and improve the solute-specific selectivity of nanofiltration (NF) membranes, we explored the ion-specific effects that govern the charge and performance of a loose polyamide NF membrane that is commonly used for solute-solute separations. Specifically, we systematically evaluated the zeta potential of the membrane under different conditions of pH, salinity, and ionic composition, and correlated the obtained data with membrane performance tested under similar conditions. Our results identify the pK_a of both carboxylic and amine groups bonded to the membrane surface and suggest that the highly polarizable chloride anions in the solution adsorb to the polyamide, increasing its negative charge. We also show that monovalent cations of different "stickiness" can neutralize the negative membrane charge to different extents due to their varying tendency to sorb to the polymer matrix or screen the fixed carboxyl groups on the membrane surface. Notably, our correlation between zeta potential measurements and permeability experiments indicates the substantial contribution of solution ions to Donnan exclusion in NF membranes.

Nanofiltration (NF) membranes have emerged as versatile tools in water treatment and other industries, allowing selective separation of solutes based on size exclusion and other molecular-level effects including Donnan exclusion, dielectric effects, and van der Waals forces[1–14]. Among these effects, it is commonly accepted that Donnan (charge) exclusion, arising from the charge of amine and carboxyl fixed groups on the surface of the polyamide active layer, plays a critical role in the separation capabilities of NF membranes[15–22]. However, questions remain regarding the effects of solution ions on the membrane charge and the consequent influence on membrane performance[23–26]; such effects can be particularly important considering recent efforts to achieve separation between similar ions[27–33]. Therefore, a molecular-level examination of the interactions between solution ions and the membrane is imperative to gain insights into membrane behavior, ultimately aiding the development of more efficient and customized NF membranes.

Measuring the zeta potential (ZP) of the membrane surface using the streaming potential method has been widely adopted to evaluate the extent and sign of membrane surface charge[34,35]. Additionally, trends of salt rejection versus pH are frequently used to explain the protonation behavior of the polyamide layer[15,36–40]. However, discrepancies in the interpretations of these measurements have been reported in the literature[34,35,38]. For instance, the minimum point of salt rejection curves is often ascribed as the isoelectric point of the membrane[41]; however, the ZP of the membrane at this supposed isoelectric point is negative for many commercial NF membranes. In another example, the literature is inconsistent in describing the effect of salt concentration on the ZP of the membrane; that is, some studies reported an increase in the negative charge of the membrane at higher salt concentrations[42], while other studies reported the opposite[38,43]. A primary goal of our research is filling these knowledge gaps.

Such discrepancies and inconsistencies in ZP measurements and interpretations suggest that NF membrane charge at a given pH is not an intrinsic (fixed) property, as it is influenced, inter alia, by the solution composition[35,44]. More specifically, membrane charge is not solely determined by the density and the pK_a values of the fixed groups, as it also depends on the specific ionic composition in the solution[45]. In this regard, different ions (including those having similar charge, valency, and hydrated radius) may differ in their stickiness[46], i.e., their ability to adsorb to the membrane surface, by substituting their hydration shell with surface groups[47], and affect its charge. Therefore, systematically exploring the effect of solution composition on the charge and performance of NF membranes can help address the aforementioned knowledge gaps and elucidate how solution composition impacts Donnan exclusion under varying conditions.

The current study systematically investigates the ZP and ion permeability of a polyamide NF membrane under a wide range of pH values, ionic

[1]Faculty of Civil and Environmental Engineering, Technion – Israel Institute of Technology, Haifa 32000, Israel. [2]Department of Civil, Environmental and Architectural Engineering, University of Colorado Boulder, Boulder, CO 80309-0428, USA. [3]These authors contributed equally: Rebecca S. Roth, Liat Birnhack. ✉e-mail: raziepsztein@technion.ac.il

compositions, and ionic strength to explore how solution ions affect the charge and performance of the membrane. Our results imply that the membrane-solution interactions are ion-specific, where "stickier" weakly hydrated ions (e.g., Cs^+) can more easily shed their hydration shell to attach to the membrane backbone and affect its charge, compared to less "sticky" strongly hydrated ions (e.g., Li^+). Additionally, we show that chlorides, which have greater polarizability than the investigated cations, can adsorb to uncharged membrane segments, enhancing the Donnan exclusion of solution anions. Overall, our work clarifies existing discrepancies in ZP studies and demonstrates the contribution of adsorbed solution ions to the charge and performance of NF membranes by correlating between ZP, the ionization behavior of the fixed groups, and ion rejection and permeability.

Results and discussion

Verification of the pK_a value of carboxyl groups on the polyamide surface

Membrane charge is directly impacted by the extent of protonation of its fixed groups, i.e., carboxylic and amine groups, a byproduct of incomplete polymerization and crosslinking of thin-film composite membranes such as the NF270 membrane[48]. Therefore, knowing the equilibrium constants (K_a) and their corresponding pK_a values for the protonation reactions of these groups (Eqs. (1) and (2)) is imperative for understanding membrane surface charge. However, the pK_a values of fixed carboxyl and amine groups bonded to polyamide membranes may differ from thermodynamic values of the acids with similar structures (i.e., ~4.2[49] and ~7.8[50,51] for benzoic acid and *N*-benzoylpiperazine, respectively), depending on the polymer chemistry. Relevant data on these acids and the polyamide structure is given in Supplementary Table 1. Our first set of experiments was therefore aimed at evaluating the pK_a values of the fixed groups bonded to the NF270 membrane and suggesting explanations for discrepancies between the membrane zeta potential (ζ) values and expected charge (Fig. 1).

$$R-COOH \leftrightarrow R-COO^- + H^+ \quad (1)$$

$$R-NH_2^+ \leftrightarrow R-NH + H^+ \quad (2)$$

A straightforward approach for determining the pK_a of the membrane's fixed groups is to analyze the membrane ζ vs. pH curve (Fig. 1a) while considering the general shape of concentration vs. pH curves of weak acid systems (Supplementary Fig. 1). Assuming that the pK_a of the carboxylic groups on the NF270 membrane is 4.5 (i.e., close to the reported pK_a of benzoic acid), a good correlation is observed between the trends of the expected concentration of the charged species (i.e., R-COO^-) and the ZP. Specifically, at pH <6.5, similar steep inclines in R-COO^- concentration (Supplementary Fig. 1a) and membrane negative charge (Fig. 1a) are observed (with the steepest incline taking place at pH 4.5), followed by steady values of both parameters at pH >6.5. This parallel behavior suggests that the pK_a of carboxylic groups on the NF270 membrane surface is around 4.5. This notion is corroborated by comparing the change in ζ with pH (Fig. 1b, closed pink circles) to the general shape of buffer capacity curve of a weak acid (Supplementary Fig. 1c), as both demonstrate a negligible change at pH far above the supposed pK_a (i.e., at pH >6.5), while the change is maximal (in absolute values) at pH = pK_a. We attribute the slight decrease in the ζ values at pH >8.5 (Fig. 1a) to dissociation of amine groups (Eq. 2), suggesting also that the density of R-NH_2^+ on the surface of the NF270 membrane is considerably lower compared to R-COO^- groups. This conclusion is reasonable since amine groups only form on the edge of the polyamide chains, while the formation of carboxyl groups can take place inside the polyamide chain[51], which is substantiated by studies quantifying functional groups on similar membranes[48,52–54]. The exact value of the pK_a of membrane amine groups is hard to locate since their density is low and there is technical difficulty in obtaining results at pH >10. Nevertheless, based on our findings (i.e., slight decrease in ζ values at pH >8.5 and a decrease in rejection at pH >10), we estimate that the pK_a of amine groups is between pH 8.5 and 9.0.

Correlation between salt rejection and zeta potential curves

Membrane charge impacts the membrane performance via Donnan (charge) exclusion, as often demonstrated by the salt rejection vs. pH curves, supposedly demonstrating good match between the pH at which the minimum rejection is achieved and the pH where minimum fixed groups on the membrane surface are charged[15,40,55,56]. However, according to previous studies (e.g., Tu et al.[57]) and the above explanation, the minimum number of charged groups on the surface of the NF270 membrane is achieved at pH

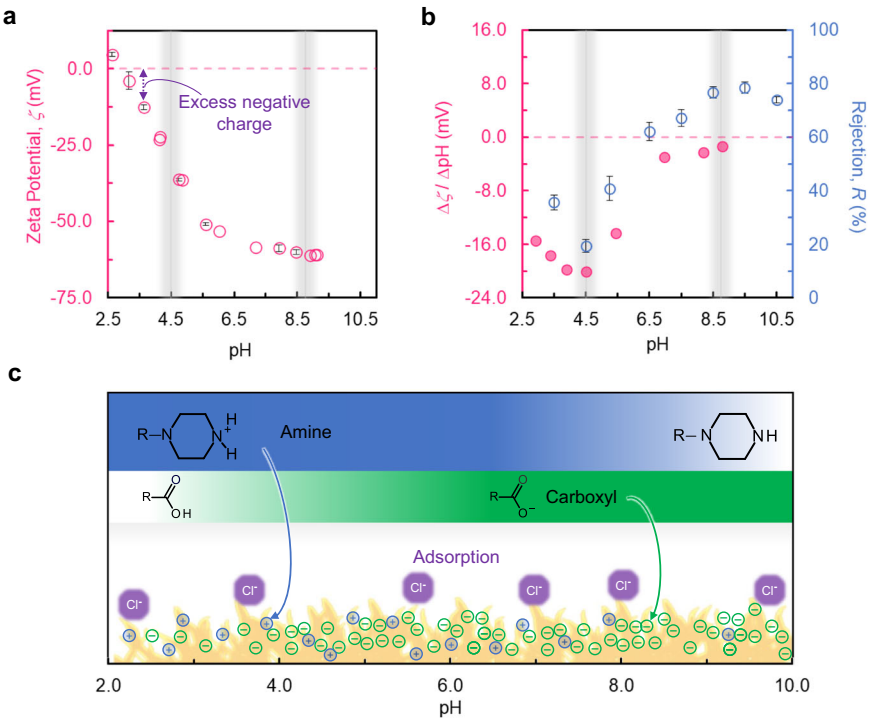

Fig. 1 | Zeta potential and performance of the NF270 membrane as a function of solution pH. **a** Average ($n = 4$) ζ of the NF270 membrane as a function of pH using 1 mM NaCl solution at 23 ± 0.8 °C (Error bars for ZP measurements that are below the order of graph point size are not shown). **b** Slope between adjacent points depicted in panel a, i.e., $\Delta\zeta$ / ΔpH (pink closed circles), and NaCl rejection (blue open circles) as a function of pH. **c** Schematics of membrane charge alteration and speciation of fixed groups with pH. Weak acids completely dissociate at pH greater (app. 2 pH units) than their pK_a values: carboxylic (green ⊖) and amine (blue ⊕) at pH > ~6 and ~10, respectively. Chloride ions are attached to neutral segments on the membrane surface, regardless of pH. Error bars in **a** and **b** represent standard deviation.

<3.0 (Fig. 1c), whereas the minimum rejection is at pH = pK_a = 4.5 (Fig. 1b, blue circles). Therefore, our results along with previously accumulated observations call for an alternative explanation for the relation between rejection vs. pH curves and membrane effective charge. Figure 1b shows an increase in rejection along the pH at 4.5 ≤ pH ≤ 9.0, which is explained by the increase in the number of deprotonated carboxyl groups at higher pH. Note that since the amine groups remain charged at pH smaller than their pK_a, the increase in the number of deprotonated carboxyl groups at pH < 9 corresponds to an increase in the overall number of charged fixed groups. However, at pH > 9 most of the amine groups are deprotonated (i.e., neutral); therefore, the membrane fixed charge becomes more negative, while the overall number of charged groups is decreased. Naturally, a decrease in the overall number of charged groups leads to a decrease in Donnan exclusion[58], which is demonstrated by a decrease in rejection of NaCl at pH > 9.0 (Fig. 1b). Notably, the decrease in rejection displayed from pH ~ 3.0 to pH 4.5 contradicts the increase in deprotonated carboxyl groups at this pH range, indicating that Donnan exclusion is not the only factor controlling the rejection at this pH range. Possibly, at pH < pK_a of the carboxyl groups, where membrane charge is minor, swelling of the polymer can outcompete the effect of charge exclusion. Thus, at pH < pK_a of the carboxyl groups, the rejection decreases with increasing pH due to increased swelling at higher pH, as previously shown for this pH range[54,59].

Irreversible and influential adsorption of chlorides

We discussed above the considerably higher density of carboxyl groups on the membrane surface compared to amine groups. Based on this idea, even under a conservative assumption of 10:1 ratio of membrane carboxyl to amine groups[42,60], at 1 pH unit below the pK_a of the carboxyl groups (i.e., pH ~3.5, in which [R – COO^-] : [R – NH_2^+] ≈ 1, Supplementary Fig. 1), ζ is presumed to be close to zero or slightly positive. Nevertheless, multiple measurements conducted in this study and previous ones[51,61,62] showed a clearly negative ζ at pH 3.5 (Fig. 1a). It was shown before that polarizable ions experience free energy minimum at the water-organic phase interface[63] and also that anions can go nearer to nonpolar or hydrophobic surfaces because they are more weakly hydrated than cations. Therefore, a likely explanation for the seemingly low membrane ζ values is Cl^- adsorption to neutral segments of the membrane surface[42] due to its enhanced "stickiness" properties (i.e., weakly hydrated and highly polarizable). Notably, earlier studies demonstrated that ions (predominantly anions) bind to the hydrophobic groups of the membranes[64–67]; our experiments conducted to further investigate this finding suggest that chloride ions better adsorb to the hydrophobic segments of the membrane, as elaborated below.

Ion concentrations in the membrane were probed using X-ray photoelectron spectroscopy (XPS) measurements for membranes that were soaked in NaCl solution (and then thoroughly rinsed with DI water), which demonstrated the adsorption of the salt ions to the membranes (Fig. 2a, b). More specifically, an increase in the intensity of both sodium and chlorine on the membrane surface was observed after soaking the polyamide membrane in NaCl solution as compared to soaking in DI water. Atomic percent calculations based on XPS survey scans showed that the chlorine atomic fraction was 5.3%, 9.3%, and 16% for samples soaked in DI water, 1 mM NaCl, and 10 mM NaCl, respectively. These data further indicate that ion sorption may be occurring in the membrane.

To further examine the hypothesis of chloride adsorption and its potential effect on Donnan exclusion, an additional set of experiments was conducted using the assumption that Cl^- adsorption onto the membrane surface is promoted at elevated temperatures[68]. More specifically, at constant salt concentration the temperature was elevated sequentially from 20 °C to 40 °C three times to test the effect of chloride adsorption on water and salt permeabilities (Fig. 2c). Our results show the irreversible effect of membrane exposure to high temperature (40 °C) at the presence of merely 1 mM NaCl. That is, increasing the temperature in the first cycle results in a lower salt permeability in the following cycles for a given temperature. We attribute this decrease in salt permeability to irreversible chloride adsorption occurring at higher temperatures, contributing to the negative charge of the membrane and therefore to enhanced Donnan exclusion in the following cycles. Notably, salt permeability at the highest temperature tested remained nearly constant over the three cycles since within the tested temperature range chloride adsorption increases with temperature during the first cycle. On the other hand, water permeability did not show a statistically significant pattern over the cycles (Supplementary Fig. 3), supporting the idea that increased charge exclusion, resulting from chloride adsorption, affected the salt permeability, as opposed to steric effects alone that affected the water permeability.

Zeta potential behavior with varying ionic strength and composition

Previous studies demonstrated contradicting effect of ionic strength (I) on membrane ZP, showing either a decline in the absolute value of ζ with increasing I[11] or the opposite[38,69]. The former observations (i.e., inverse relationships) are explained by charge screening, while the latter imply that adsorption of solution ions (e.g., chlorides) to the membrane surface may occur. To elucidate such phenomena, the effect of I (or salt concentration) on ζ was examined at different pH and using different types of cations (Fig. 3a–c).

Our results show that for ionic strength higher than 1 mM (regardless of the tested cation or the pH), higher salt concentration resulted in better charge screening and thus reduced absolute value of ZP (|ζ|, Fig. 3a–c). However, further examination of the effect of solution ions on ZP at low I conditions (<1 mM) demonstrates a different trend where increasing I leads to a decreased ζ, suggesting that adsorption of Cl^- ions to uncharged segments of the membrane is a prominent factor for highly diluted solutions.

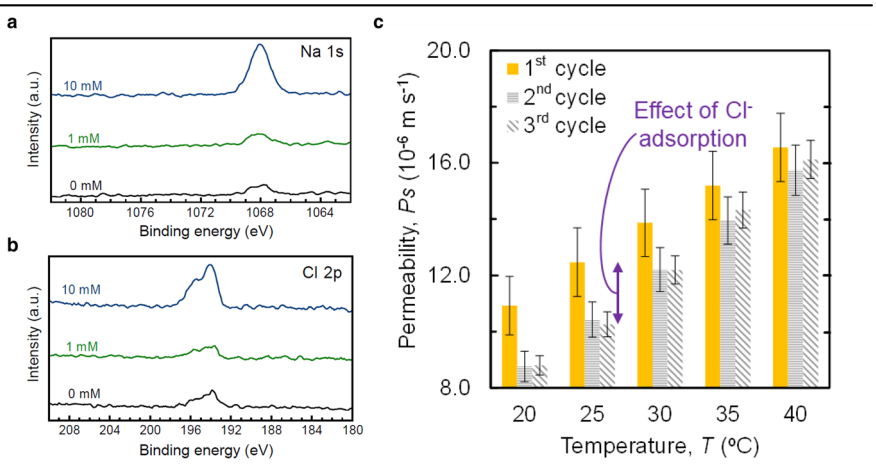

Fig. 2 | Irreversible and influential adsorption of chlorides. a, **b** X-ray photoelectron spectroscopy core scans of sodium 1s and chlorine 2p for membranes soaked in 0 mM, 1 mM, and 10 mM sodium chloride. Samples were soaked in their respective solutions for 24 hr at 40 °C and thoroughly rinsed in DI water. **c** Three consecutive experiments examining NaCl permeability as a function of temperature (i.e., in each cycle, the temperature was elevated from 20 °C to 40 °C) to explore chloride irreversible adsorption. The same membrane coupons were used throughout the three experiments. Experimental conditions: 1 mM NaCl, applied pressure of 18 bar, and crossflow velocity of 2.13 m s^{-1}. Error bars in **c** represent standard deviation.

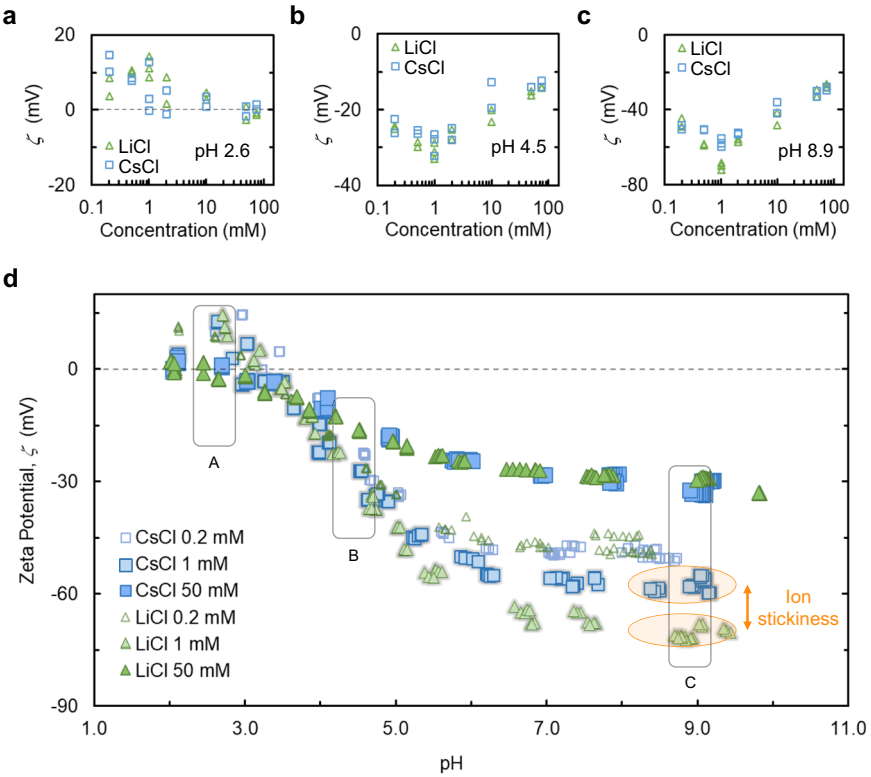

Fig. 3 | Effects of specific conditions on the zeta potential of the NF270 membrane. The membrane was in contact with single-salt solutions of CsCl (blue squares) or LiCl (green triangles) at various concentrations and pH values. **a**–**c** Average ($n = 4$) ζ obtained for solutions of different concentrations of CsCl and LiCl at 21 ± 2 °C and pH 2.62 ± 0.15, pH 4.51 ± 0.02, and pH 8.9 ± 0.37, respectively. **d** The stickiness tendency of Cs^+ (compared to Li^+) is noticeable only for 1 mM solutions (glowing symbols) at pH > 5.5. At high ionic strength, the $|\zeta|$ is lower as the electric double layer is compressed.

Table 1 | Main properties of the ions examined in this work

Ion	Crystal radius (Å)[80]	Hydrated radius (Å)[80]	Hydration enthalpy (kcal mol^{-1})[81]	Polarizability (Å^3)[82]
Lithium (Li^+)	0.60	3.82	−126.8	0.029
Sodium (Na^+)	0.95	3.58	−99.29	0.18
Potassium (K^+)	1.33	3.31	−78.95	0.81
Cesium (Cs^+)	1.69	3.29	−66.99	2.02
Chloride (Cl^-)	1.81	3.32	−76.04	3.5
Hydronium (H_3O^+)	–	2.82	–	1.19
Hydroxide (OH^-)	1.76	3.00	−124.3	1.91
Bicarbonate (HCO_3^-)	1.78[83]	4.39[84]	−90.8	–
Carbonate (CO_3^{-2})	2.66	3.94	−333.4	–

For consistency, data was collected from the same source for a specific parameter, unless otherwise mentioned.

More specifically, under the conditions of negatively charged fixed groups (i.e., pH ≥ 4.5, Fig. 3b, c) and very low salt concentrations (i.e., $I < 1$ mM), chlorides stick to the membrane surface to higher extent than the cations[42], presumably due to the higher polarizability (and therefore "stickiness") of chlorides compared to the cations (Table 1). As a result, elevated membrane negative charge (i.e., lower ζ) is attained by elevating the concentration of Cl^- in the solution. At higher salinities ($I > 1$ mM), however, it is likely that chloride adsorption reaches its maximum and charge screening by the solution cations becomes prominent, leading to a decrease in the absolute value of ζ. Notably, at concentration of 50 mM, charge screening is considerable regardless of the cation, resulting in identical ζ for both cation solutions.

To support the effect of Cl^- adsorption on membrane charge at low salinities, the effect of I on ζ was examined at pH 2.6 (Fig. 3a), where membrane fixed groups are slightly positive and therefore both phenomena (i.e., charge screening and chloride adsorption) are expected to impact ζ in the same manner. Figure 3a shows a consistent trend of decrease in ζ with the increase of I, corroborating the hypothesis of Cl^- adsorption being the prominent factor effecting ZP at low salinities.

It was recently shown that even ions possessing similar hydrated size and charge such as Li^+ and Cs^+ show different permeabilities through NF membranes[37,70–72]. Such differences in the transmembrane permeation of similar ions stem from delicate and more complex molecular-level interactions beyond simple size and charge exclusion[71,73,74]. Similarly, the differences in "stickiness" of Li^+ and Cs^+ can explain the different ζ values attained with CsCl and LiCl solutions (Fig. 3d). Noticeably, at high pH (>6) the CsCl solution has a less negative ζ than LiCl, which can be attributed to Cs^+ 's softer hydration shell (or lower hydration enthalpy, i.e., $|\Delta H_{hyd}(Cs^+)| < |\Delta H_{hyd}(Li^+)|$, Table 1), which facilitates its increased adsorption to the surface compared to Li^+. In particular, our results demonstrate that the differences in the ZP values achieved with similar ions are most noticeable for moderate concentrations (between 0.5 and 1 mM). At high concentrations (50 mM), similar ZP values were measured for LiCl and CsCl presumably due to the screening effect at higher concentrations that outcompetes ion-specific effects. We note that the differences in the stickiness of the ions have only a slight impact on the membrane ζ values. Thus, only considerable differences in stickiness (such as between Li^+ and Cs^+) are noticeable, while similar cations (e.g., K^+ and Cs^+ or Li^+ and Na^+) show insignificant differences in ζ values (Supplementary Fig. 4).

Correlation between membrane zeta potential and ion permeability

It was shown that ZP is not an indicator of the fixed membrane charge alone, but also represents contribution from the solution ions. In other words, ZP represents the effective charge of the membrane, which is the charge experienced by the solution at the vicinity of the membrane resulting from the combination of the charge of the membrane fixed groups and solution

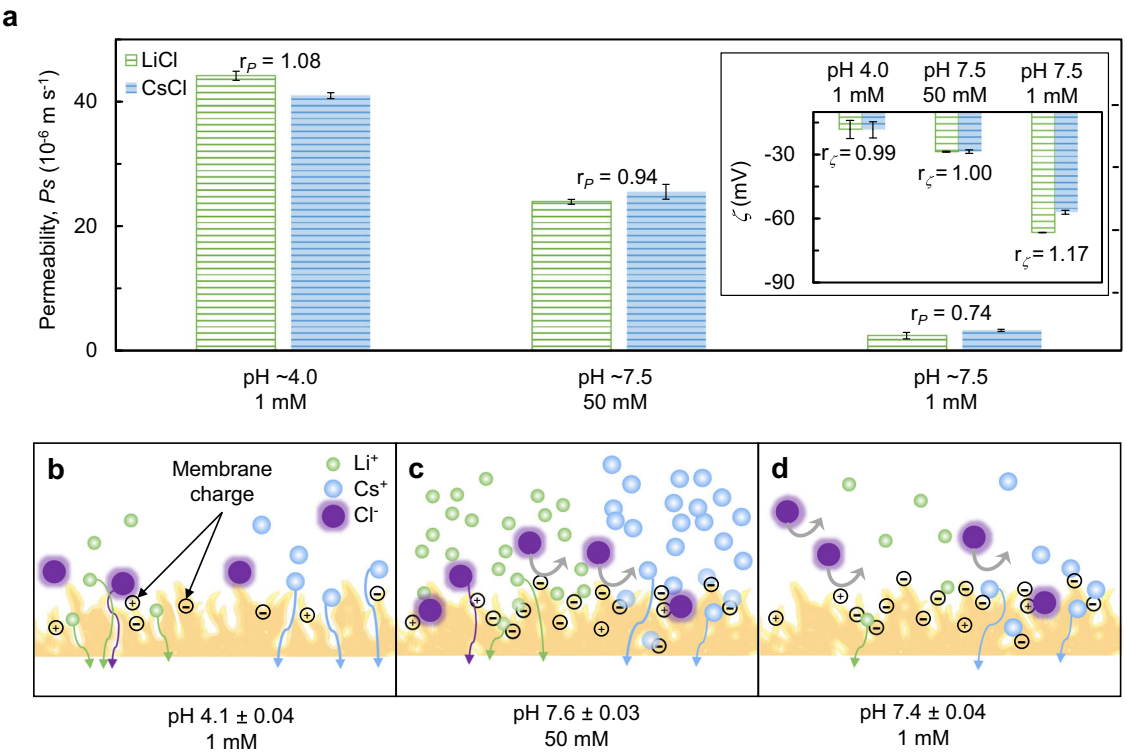

Fig. 4 | Correlation between membrane zeta potential and ion permeability. **a** LiCl (green) and CsCl (blue) permeabilities at different conditions and the respective ζ (inset). Experimental conditions during the permeability tests: 5 bar (72.5 psi), 24.8 ± 0.1 °C, and crossflow velocity of 2.13 m s^{-1}. Ratios between LiCl and CsCl measurements of ζ and P_s, r_ζ and r_P, respectively, are indicated next to the bars of each condition. Donnan effect on ion permeation at **b** pH 4.0 and low ionic strength; **c** pH 7.5 and high ionic strength; and **d** pH 7.5 and low ionic strength. Membrane charge is indicated by black ⊕/⊖ circles.

ions. Therefore, it is reasonable that ZP is a good indicator for Donnan exclusion, which is also a result of the effective charge rather than the fixed charge of the membrane alone. To better understand to what extent ZP is a predictor for Donnan exclusion, the correlations between ZP and ion permeability were examined for chloride salts of Li^+ and Cs^+ representing ions of low and high stickiness (Table 1), respectively (Fig. 4a). In addition, I and pH were altered to examine salt permeability under various known ζ values (inset of Fig. 4a).

Our results show a clear inverse correlation between the parameters; that is, salt permeability is reduced with the increase in $|\zeta|$, which implies that ZP is a reasonable indicator for Donnan exclusion. For instance, at pH 4.0 and I = 1 mM, the $|\zeta|$ is relatively low due to weak membrane charge with the accompanying reduced Donnan effects, which results in relatively high ion permeability (Fig. 4b). At pH 7.5 and high ionic strength, the $|\zeta|$ is greater and consequently ion permeability is reduced. The main reason for the lower permeability under these conditions is schematically explained in Fig. 4c, showing higher membrane charge, which is partly neutralized by the ions. At pH 7.5 and low ionic strength (Fig. 4d), there is limited charge screening, therefore many membrane charges generate strong Donnan effects resulting in very low permeability. The ZP results may also imply subtle differences in Donnan exclusion experienced by Li^+ and Cs^+, as reflected by the good correlation between the ratios of LiCl and CsCl ζ ($r_\zeta = \zeta_{LiCl}/\zeta_{CsCl}$) and P_s ($r_P = P_s(LiCl)/P_s(CsCl)$). Notably, the largest r_ζ was obtained at pH 7.5 and 1 mM, where the negative membrane charge is high (Fig. 1a, c) and charge screening is minor (Fig. 4d), leading to noticeable differences in Cs^+ and Li^+ permeabilities (r_P = 0.74). It is stressed that we tested the match between ZP and Donnan exclusion only for pH ≤ 7.5, where the fixed membrane charge is solely influenced by protonation of carboxyl groups (Eq. (1)), while the amine groups are positively charged throughout the pH range. Thus, in the tested conditions, ZP is directly related to the overall number of charged fixed groups. On the other hand, at pH > 7.5, the increase in $|\zeta|$ with pH is the outcome of the protonation of charged amine groups (i.e., Eq. (2)), resulting in a decrease in overall number of charged groups, but an increase in the overall negative charge. Lastly, we considered the potential effect of the carbonate system and water ions on the pH near the membrane wall. Based on the pK_a values, the concentrations of the various species (Supplementary Table 3), and the expected permeability of the species, we computed the potential effect on the pH (e.g., Supplementary Fig. 2). These calculations showed the minor effect of the carbonate system and water ions on our results.

Discussion

Understanding the effects of solution ions on Donnan exclusion and transport through NF membranes can aid growing efforts to improve the solute-specific selectivity of NF membranes. Motivated by knowledge gaps in previous research using ZP to study membrane surface charge, we systematically evaluated membrane ZP over a range of pH, salinity, and ionic composition and corelated the results to membrane permeability tested under similar conditions. Initially, we determined the pK_a of carboxyl and amine groups to be ~4.5 and ~8.5, respectively. We then proceeded to explain how increased swelling accounts for the discrepancy between the isoelectric point assumed at the minimum point of salt rejection curves and the isoelectric point measured by ZP analysis. We also explain how chloride adsorption accounts for membranes' charge remaining negative despite the pK_a of its functional groups indicating it should be positive. We then systematically evaluated membrane ZP over a range of pH, salinity, and ionic composition to reconcile conflicting reports of the effect of solution concentration on ZP. More specifically, chloride adsorption can explain the increase in ZP absolute value with increasing solution concentration until the point of saturation of bonding sites on the polymer backbone, after which condensing of the electric double layer accounts for decreasing the absolute value of ZP. We conclude with demonstrating that Cs^+ ions, with lower hydration enthalpy (and therefore higher stickiness), adsorb more easily to the membrane surface than Li^+ ions and showing how ZP is a good

indicator of Donnan exclusion, which is evidenced in permeability experiments.

Methods

Membranes and chemicals

Analytical grade chloride-based salts of alkali metals including lithium (LiCl), sodium (NaCl), potassium (KCl), and cesium (CsCl) were purchased from Acros Organics, BioLab, Merck, and Fisher Chemicals, respectively. The ions constituting these salts systematically differ in several properties that can affect the ability of the ions to adsorb to the membrane surface and affect its charge (Table 1). Single-salt solutions for ZP measurements and for NF filtration tests were prepared by dissolving the powdered salt in ultrapure water (Merck, <0.055 mS cm^{-1}) and deionized water (DI) (Zailon, <0.8 mS cm^{-1}), respectively. Hydrochloric acid (HCl) and sodium hydroxide (NaOH) at concentrations of 0.05 M were used to adjust the solution pH. Flat sheets of a thin film composite NF membrane (NF270, Dow Filmtec) were used for all experiments. This membrane is considered a "loose" NF membrane[75], where charge effects possess a critical role in the separation[54,57,76]. All membrane coupons were pretreated with a 25% v/v isopropyl alcohol solution for 30 min and then rinsed with deionized water for 30 min, three times. Each membrane coupon was used for a single experiment of ZP or filtration (i.e., each experiment was performed with different coupons except for the experiment described in Fig. 2c).

Zeta potential measurements

Membrane surface charge was evaluated by measuring streaming potential using the SurPASS3 electro kinetic analyzer for solid surface analysis (Anton Paar GmbH, Austria). The streaming potential is converted to zeta potential using the Helmholtz–Smoluchowsi equation:

$$\zeta = \frac{dU_{str}}{dp}\frac{\eta}{\varepsilon_r \cdot \varepsilon_0}\frac{L}{A \cdot R} \quad (3)$$

where ζ is the zeta potential, U_{str} is the streaming potential, p is the applied hydraulic pressure, η is the liquid viscosity, ε_r is the liquid permittivity, ε_0 is the permittivity in vacuum, R is the electrical resistance across the medium, and L and A are the length and cross-sectional area of the channel, respectively.

Four chloride-based single salt solutions (LiCl, NaCl, KCl, and CsCl) at concentrations of 0.1, 0.2, 0.5, 1, 2, 10, 50, and 75 mM were used during the ZP measurements. For each solution, stabilization of the measurements was first obtained at the initial pH (i.e., around pH 6.0). Next, the pH was elevated to pH 9.0 by injecting NaOH and gradually reduced towards pH 2.5, while measuring the ZP at intervals of around 0.5 pH unit. All experiments were performed at room temperature (23 ± 3 °C) with a continuous degassing of carbon dioxide from the solution by bubbling N_2 gas into the beaker from which the solution is pumped to the measuring cell. The cell gap was adjusted to 100 ± 10 um and the following criteria were verified for ensuring reliable results: correlation coefficient (linearity of the streaming potential vs pressure ramp) >0.989 [-], absolute value of Asymmetry <10 mV, and static resistance <10^4 kOhm.

X-ray photoelectron spectroscopy measurements

X-ray photoelectron spectra were acquired with a Kratos Supra X-ray photo electron spectrometer. Dow NF270 membrane samples were soaked for 24 h in DI water or 1 mM NaCl solution at 40 °C, rinsed with DI water, and then soaked in DI water at room temperature for at least 6 h. Prior to testing, samples were left to dry in ambient conditions overnight. Survey spectra were used to calculate the element atomic percent on the surface and high-resolution spectra provided information on elemental chemical state. The Al K alpha X-ray source was operated at 1486.69 kV and 15.00 mA current emission. Survey spectra were acquired from 1200 eV to 0 eV at a resolution of 160, while high resolution scan ranges were based off the element being analyzed and a resolution of 20.

Nanofiltration tests

The experimental setup used for the permeability and rejection tests is operated in a crossflow mode and consists of a 10 L feed tank, high pressure pump, and three custom-made stainless steel cells accommodating the 15.3 cm^2 flat-sheet membrane coupons. The reject and permeate streams of the three cells were continuously drawn back to the feed tank. The applied pressure, crossflow velocity, feed pH, and temperature were continuously monitored and maintained constant unless otherwise mentioned. In each experiment, following the alteration of the feed property, i.e., temperature, salt concentration, or pH, the system was allowed to stabilize for 30 minutes before permeate samples were taken. Prior to each experiment, the membrane coupons were compacted overnight with DI water by applying a pressure higher than the operation pressure by at least 2 bar.

Single-salt solutions were used for each experiment, so that salt concentrations in the feed and permeate streams (C_F and C_P, respectively, mol L^{-1}) were deduced from electrical conductivity measurements (Eutech Instruments, CON2700). In addition, the weight of the permeate stream collected over a given time was used for calculating J_W (L m^{-2} h^{-1}), the water flux through the membrane, from which J_s (=$J_W \cdot C_P$), the salt flux, was also calculated. Concentration polarization was taken into consideration using the film theory[77,78]:

$$C_m = \left(C_f - C_p\right)\exp\left(\frac{J_W}{k}\right) + C_p \quad (4)$$

where, C_m, (mol L^{-1}) is the salt concentration on the membrane wall of the feed side; k is the mass transfer coefficient (m s^{-1}) computed based on Sherwood correlation for turbulent flow in rectangular channel[79] and parameters in Supplementary Table 2. Water permeability, P_W, and salt permeability, P_s (m s^{-1}), were calculated for each membrane cell using the solution-diffusion model:

$$P_W = \frac{J_W}{\triangle P - \triangle \pi} \quad (5)$$

$$P_S = \frac{J_s}{C_m - C_p} \quad (6)$$

where ΔP and $\Delta \Pi$ are the pressure gradient and osmotic pressure gradient across the membrane, respectively.

Data availability

The datasets generated during and/or analyzed during the current study are available from the corresponding author on reasonable request.

Received: 30 July 2023; Accepted: 21 March 2024;
Published online: 30 March 2024

References

1. Zhao, Y. et al. Differentiating Solutes with Precise Nanofiltration for Next Generation Environmental Separations: A Review. *Environ. Sci. Technol.* https://doi.org/10.1021/acs.est.0c04593 (2021)
2. Mohammad, A. W. et al. Nanofiltration membranes review: Recent advances and future prospects. *Desalination* **356**, 226–254 (2015).
3. Villalobos, L. F., Zhang, J. & Elimelech, M. Nanofiltration for circularity: Fit-for-purpose design and evaluation. *One Earth* **6**, 767–771, https://doi.org/10.1016/j.oneear.2023.06.007 (2023).
4. Liang, Y. et al. Polyamide nanofiltration membrane with highly uniform sub-nanometre pores for sub-1 Å precision separation. *Nat. Commun.* **11**, 1–9 (2020).
5. Jia, T. Z. et al. Recent advances in nanofiltration-based hybrid processes. *Desalination* **565**, https://doi.org/10.1016/j.desal.2023.116852 (2023).
6. Chen, X., Boo, C. & Yip, N. Y. Influence of Solute Molecular Diameter on Permeability-Selectivity Tradeoff of Thin-Film Composite

Polyamide Membranes in Aqueous Separations. *Water Res.* **201**, 117311 (2021).
7. Zheng, J. et al. Selective removal of heavy metals from saline water by nanofiltration. *Desalination* **525**, 115380 (2022).
8. Szymczyk, A. & Fievet, P. Investigating transport properties of nanofiltration membranes by means of a steric, electric and dielectric exclusion model. *J. Memb. Sci.* **252**, 77–88 (2005).
9. Iddya, A. et al. A reverse-selective ion exchange membrane for the selective transport of phosphates via an outer-sphere complexation–diffusion pathway. *Nat. Nanotechnol.* **17**, 1222–1228 (2022).
10. Freger, V. Ion partitioning and permeation in charged low-T* membranes. *Adv. Colloid Interfac.* **277**, https://doi.org/10.1016/j.cis.2020.102107 (2020).
11. Ahmad, N. N. R., Ang, W. L., Teow, Y. H., Mohammad, A. W. & Hilal, N. Nanofiltration membrane processes for water recycling, reuse and product recovery within various industries: A review. *J. Water Process Eng.* **45**, 102478 (2022).
12. Van Der Bruggen, B. & Vandecasteele, C. Removal of pollutants from surface water and groundwater by nanofiltration: overview of possible applications in the drinking water industry. *Environ. Pollut.* **122**, 435–445 (2003).
13. Wang, J. et al. A critical review of transport through osmotic membranes. *J. Memb. Sci.* **454**, 516–537 (2014).
14. Wang, R., Zhang, J., Tang, C. Y. & Lin, S. Understanding Selectivity in Solute–Solute Separation: Definitions, Measurements, and Comparability. *Environ. Sci. Technol.* **56**, 2605–2616 (2022).
15. Mänttäri, M., Pihlajamäki, A. & Nyström, M. Effect of pH on hydrophilicity and charge and their effect on the filtration efficiency of NF membranes at different pH. *J. Memb. Sci*. **280**, 311–320 (2006).
16. Gao, Y., Zhao, Y., Wang, X. M., Tang, C. & Huang, X. Modulating the Asymmetry of the Active Layer in Pursuit of Nanofiltration Selectivity via Differentiating Interfacial Reactions of Piperazine. *Environ. Sci. Technol.* **56**, 14038–14047 (2022).
17. Léniz-Pizarro, F., Liu, C., Colburn, A., Escobar, I. C. & Bhattacharyya, D. Positively charged nanofiltration membrane synthesis, transport models, and lanthanides separation. *J. Memb. Sci.* **620**, 118973 (2021).
18. Freger, V. & Ramon, G. Z. Polyamide desalination membranes: Formation, structure, and properties. *Prog. Polym. Sci*. **122**, https://doi.org/10.1016/j.progpolymsci.2021.101451 (2021).
19. Lu, X. & Elimelech, M. Fabrication of desalination membranes by interfacial polymerization: History, current efforts, and future directions. *Chem. Soc. Rev.* **50**, 6290–6307 (2021).
20. Xu, P. et al. Fabrication of highly positively charged nanofiltration membranes by novel interfacial polymerization: Accelerating Mg2+ removal and Li+ enrichment. *J. Memb. Sci*. **668**, 121251 (2023).
21. Foo, Z. H., Rehman, D., Bouma, A. T., Monsalvo, S. & Lienhard, J. H. Lithium Concentration from Salt-Lake Brine by Donnan-Enhanced Nanofiltration. *Environ. Sci. Technol.* **57**, 6320–6330 (2023).
22. He, R. et al. Unprecedented Mg2+/Li+ separation using layer-by-layer based nanofiltration hollow fiber membranes. *Desalination* **525**, 115492 (2022).
23. Blankert, B., Huisman, K. T., Martinez, F. D., Vrouwenvelder, J. S. & Picioreanu, C. Are commercial polyamide seawater and brackish water membranes effectively charged? *J. Memb. Sci. Lett*. **2**, 100032 (2022).
24. Stolov, M. & Freger, V. Ion transport and specificity in polyamide membranes studied by conductivity and its activation energy. *J. Memb. Sci*. **678**, 121616 (2023).
25. Boussouga, Y. A., Than, H. & Schäfer, A. I. Selenium species removal by nanofiltration: Determination of retention mechanisms. *Sci. Tot Environ.* **829**, 154287 (2022).
26. Zelner, M. et al. Elucidating ion transport mechanism in polyelectrolyte-complex membranes. *J. Memb. Sci.* **658**, 120757 (2022).
27. Lu, J. et al. An artificial sodium-selective subnanochannel. *Sci. Adv*. **9**, eabq1369 (2023).
28. Warnock, S. J. et al. Engineering Li/Na selectivity in 12-Crown-4–functionalized polymer membranes. *Proc. Natl Acad. Sci.* **118**, e2022197118 (2021).
29. Duchanois, R. M., Porter, C. J., Violet, C., Verduzco, R. & Elimelech, M. Membrane Materials for Selective Ion Separations at the Water – Energy Nexus. *Adv. Mater.* **2101312**, 1–18 (2021).
30. Epsztein, R., DuChanois, R. M., Ritt, C. L., Noy, A. & Elimelech, M. Towards single-species selectivity of membranes with subnanometre pores. *Nat. Nanotechnol.* **15**, 426–436 (2020).
31. DuChanois, R. M. et al. Designing polymeric membranes with coordination chemistry for high-precision ion separations. *Sci. Adv*. **8**, 1–10 (2022).
32. Tang, C. & Bruening, M. L. Ion separations with membranes. *J. Polym. Sci.* **58**, 2831–2856 (2020).
33. Epsztein, R. Intrinsic limitations of nanofiltration membranes to achieve precise selectivity in water-based separations. *Front. Membr. Sci. Technol*. **1**, 1048416 (2022).
34. Hagmeyer, G. & Gimbel, R. Modelling the rejection of nanofiltration membranes using zeta potential measurements. *Sep. Purif. Technol*. **15**, 19–30 (1999).
35. Ernst, M., Bismarck, A., Springer, J. & Jekel, M. Zeta-potential and rejection rates of a polyethersulfone nanofiltration membrane in single salt solutions. *J. Memb. Sci.* **165**, 251–259 (2000).
36. Epsztein, R., Shaulsky, E., Dizge, N., Warsinger, D. M. & Elimelech, M. Role of Ionic Charge Density in Donnan Exclusion of Monovalent Anions by Nanofiltration. *Environ. Sci. Technol.* **52**, 4108–4116 (2018).
37. Epsztein, R., Cheng, W., Shaulsky, E., Dizge, N. & Elimelech, M. Elucidating the mechanisms underlying the difference between chloride and nitrate rejection in nanofiltration. *J. Memb. Sci*. https://doi.org/10.1016/j.memsci.2017.10.049 (2018)
38. Jun, B.-M. et al. Charge characteristics (surface charge vs. zeta potential) of membrane surfaces to assess the salt rejection behavior of nanofiltration membranes. *Sep. Purif. Technol*. **247**, 117026 (2020).
39. Nilsson, M., Trägårdh, G. & Östergren, K. The influence of pH, salt and temperature on nanofiltration performance. *J. Memb. Sci*. **312**, 97–106 (2008).
40. Shefer, I., Peer-Haim, O., Leifman, O. & Epsztein, R. Enthalpic and Entropic Selectivity of Water and Small Ions in Polyamide Membranes. *Environ. Sci. Technol.* **55**, 14863–14875 (2021).
41. Shefer, I., Lopez, K., Straub, A. P. & Epsztein, R. Applying Transition-State Theory to Explore Transport and Selectivity in Salt-Rejecting Membranes: A Critical Review. *Environ. Sci. Technol*. **56**, https://doi.org/10.1021/acs.est.2c00912 (2022).
42. Elimelech, M., Chen, W. H. & Waypa, J. J. Measuring the zeta (electrokinetic) potential of reverse osmosis membranes by a streaming potential analyzer. *Desalination* **95**, 269–286 (1994).
43. Coday, B. D. et al. Indirect determination of zeta potential at high ionic strength: Specific application to semipermeable polymeric membranes. *J. Memb. Sci.* **478**, 58–64 (2015).
44. Childress, A. E. & Elimelech, M. Effect of solution chemistry on the surface charge of polymeric reverse osmosis and nanofiltration membranes. *J. Memb. Sci.* **119**, 253–268 (1996).
45. Burns, D. B. & Zydney, A. L. Buffer Effects on the Zeta Potential of Ultrafiltration Membranes. *J. Memb. Sci*. **172**, 39–48 (2000).
46. Collins, K. D. Sticky ions in biological systems. *Proc. Natl Acad. Sci. USA* **92**, 5553–5557 (1995).
47. Leontidis, E., Christoforou, M., Georgiou, C. & Delclos, T. The ion-lipid battle for hydration water and interfacial sites at soft-matter interfaces. *Curr. Opin. Colloid. Interface Sci.* **19**, https://doi.org/10.1016/j.cocis.2014.02.003 (2014).

48. Coronell, O., González, M. I., Mariñas, B. J. & Cahill, D. G. Ionization behavior, stoichiometry of association, and accessibility of functional groups in the active layers of reverse osmosis and nanofiltration membranes. *Environ. Sci. Technol.* **44**, 6808–6814 (2010).
49. Zevatskii, Y. E. & Lysova, S. S. Empirical procedure for the calculation of ionization constants of organic compounds in water from their molecular volume. *Russ. J. Org. Chem.* **45**, 825–834 (2009).
50. Hall, H. K. Correlation of the Base Strengths of Amines. *J. Am. Chem. Soc.* **79**, 5441–5444 (1957).
51. Fernández, J. F., Jastorff, B., Störmann, R., Stolte, S. & Thöming, J. Thinking in terms of structure-activity-relationships (T-SAR): A tool to better understand nanofiltration membranes. *Membranes* **1**, 162–183 (2011).
52. Chen, D., Werber, J. R., Zhao, X. & Elimelech, M. A facile method to quantify the carboxyl group areal density in the active layer of polyamide thin-film composite membranes. *J. Memb. Sci*. **534**, 100–108 (2017).
53. Coronell, O., Mariñas, B. J., Zhang, X. & Cahill, D. G. Quantification of functional groups and modeling of their ionization behavior in the active layer of FT30 reverse osmosis membrane. *Environ. Sci. Technol.* **42**, 5260–5266 (2008).
54. Ritt, C. L. et al. Ionization behavior of nanoporous polyamide membranes. *Proc. Natl Acad. Sci. USA* **117**, 30191–30200 (2020).
55. Luo, J. & Wan, Y. Effects of pH and salt on nanofiltration-a critical review. *J. Memb. Sci.* **438**, https://doi.org/10.1016/j.memsci.2013.03.029 (2013).
56. Peer-Haim, O., Shefer, I., Singh, P., Nir, O. & Epsztein, R. The Adverse Effect of Concentration Polarization on Ion-Ion Selectivity in Nanofiltration. *Environ. Sci. Technol. Lett.* https://doi.org/10.1021/acs.estlett.3c00124 (2023)
57. Tu, K. L., Nghiem, L. D. & Chivas, A. R. Coupling effects of feed solution pH and ionic strength on the rejection of boron by NF/RO membranes. *Chem. Eng. J.* **168**, 700–706 (2011).
58. Luo, J. & Wan, Y. Mix-charged nanofiltration membrane: Engineering charge spatial distribution for highly selective separation. *Chem. Eng. J*. **464**, https://doi.org/10.1016/j.cej.2023.142689 (2023).
59. Zhao, C., Nie, S., Tang, M. & Sun, S. Polymeric pH-sensitive membranes - A review. *Prog. Polym. Sci.* **36**, https://doi.org/10.1016/j.progpolymsci.2011.05.004 (2011).
60. Coronell, O., Mariñas, B. J. & Cahill, D. G. Depth heterogeneity of fully aromatic polyamide active layers in reverse osmosis and nanofiltration membranes. *Environ. Sci. Technol.* **45**, 4513–4520 (2011).
61. Giagnorio, M. et al. Achieving low concentrations of chromium in drinking water by nanofiltration: membrane performance and selection. *Environ. Sci. Pollut. R.* **25**, 25294–25305 (2018).
62. Imbrogno, A. et al. Organic fouling control through magnetic ion exchange-nanofiltration (MIEX-NF) in water treatment. *J. Memb. Sci*. **549**, 474–485 (2018).
63. Wick, C. D., Kuo, I. F. W., Mundy, C. J. & Dang, L. X. The effect of polarizability for understanding the molecular structure of aqueous interfaces. *J. Chem. Theory Comput.* **3**, 2002–2010 (2007).
64. Wadekar, S. S. & Vidic, R. D. Insights into the rejection of barium and strontium by nanofiltration membrane from experimental and modeling analysis. *J. Memb. Sci.* **564**, 742–752 (2018).
65. Pino-Soto, L. et al. Influence of multivalent-electrolyte metal solutions on the superficial properties and performance of a polyamide nanofiltration membrane. *Sep. Purif. Technol.* **272**, 118846 (2021).
66. Déon, S., Escoda, A. & Fievet, P. A transport model considering charge adsorption inside pores to describe salts rejection by nanofiltration membranes. *Chem. Eng. Sci.* **66**, 2823–2832 (2011).
67. Bruni, L. & Bandini, S. The role of the electrolyte on the mechanism of charge formation in polyamide nanofiltration membranes. *J. Memb. Sci*. **308**, 136–151 (2008).
68. Zhou, X. et al. Intrapore energy barriers govern ion transport and selectivity of desalination membranes. *Sci. Adv.* **6**, 1–10 (2020).
69. Rho, H., Chon, K. & Cho, J. Surface charge characterization of nanofiltration membranes by potentiometric titrations and electrophoresis: Functionality vs. zeta potential. *Desalination* **427**, 19–26 (2018).
70. Santafé-Moros, A., Gozálvez-Zafrilla, J. M. & Lora-García, J. Nitrate removal from ternary ionic solutions by a tight nanofiltration membrane. *Desalination* **204**, 63–71 (2007).
71. Lu, C. et al. Dehydration-enhanced ion-pore interactions dominate anion transport and selectivity in nanochannels. *Sci. Adv.* **9**, eadf8412 (2023).
72. Pavluchkov, V., Shefer, I., Peer-Haim, O., Blotevogel, J. & Epsztein, R. Indications of ion dehydration in diffusion-only and pressure-driven nanofiltration. *J. Memb. Sci.* **648**, 120358 (2022).
73. Shefer, I., Peer-Haim, O. & Epsztein, R. Limited ion-ion selectivity of salt-rejecting membranes due to enthalpy-entropy compensation. *Desalination* **541**, 116041 (2022).
74. Richards, L. A., Richards, B. S., Corry, B. & Schäfer, A. I. Experimental energy barriers to anions transporting through nanofiltration membranes. *Environ. Sci. Technol.* **47**, 1968–1976 (2013).
75. Freger, V. Swelling and morphology of the skin layer of polyamide composite membranes: An atomic force microscopy study. *Environ. Sci. Technol.* **38**, 3168–3175 (2004).
76. Boussu, K. et al. Characterization of polymeric nanofiltration membranes for systematic analysis of membrane performance. *J. Memb. Sci*. **278**, 418–427 (2006).
77. Gekas, V. & Hallström, B. Mass transfer in the membrane concentration polarization layer under turbulent cross flow. I. Critical literature review and adaptation of existing sherwood correlations to membrane operations. *J. Memb. Sci*. **30**, 153–170 (1987).
78. Oren, Y. S., Freger, V. & Nir, O. New compact expressions for concentration-polarization of trace-ions in pressure-driven membrane processes. *J. Memb. Sci. Lett.* **1**, 100003 (2021).
79. Mulder, M. H. V. Polarization phenomena and membrane fouling. *Membrane Sci. Technol.* **2**, 45–84 (1995).
80. Nightingale, E. R. Phenomenological theory of ion solvation. Effective radii of hydrated ions. *J. Phys. Chem.* **63**, 1381–1387 (1959).
81. Marcus, Y. A simple empirical model describing the thermodynamics of hydration of ions of widely varying charges, sizes, and shapes. *Biophys. Chem.* **51**, https://doi.org/10.1016/0301-4622(94)00051-4 (1994).
82. Molina, J. J. et al. Ions in solutions: Determining their polarizabilities from first-principles. *J. Chem. Phys.* **134**, 014511 (2011).
83. Hussain, A. et al. Ion Transport Behavior in Bipolar Membrane Electrodialysis: Role of Anions. *Ind. Eng. Chem. Res.* **62**, 698–707 (2023).
84. Geise, G. M. et al. Specific ion effects on membrane potential and the permselectivity of ion exchange membranes. *Phys. Chem. Chem. Phy.* **16**, 21673–21681 (2014).

Acknowledgements

This research was supported by the Israel Science Foundation (grant No. 1269/21) and a grant from the United States – Israel Binational Science Foundation (BSF), Jerusalem, Israel (grant No. 2021615), and the United States National Science Foundation (Award No. CBET 2136835).

Author contributions

The manuscript was written with the contributions of all authors. All authors have given approval for the final version of the manuscript. R.S.R. and L.B. contributed equally to this work. R.S.R., L.B., M.A. and E.A.H. designed and executed the experiments, and analyzed the results. A.P.S. designed and guided the experiments and analyzed the results. R.E. designed and guided the experiments, analyzed the results, and led the research.

Competing interests
The authors declare no competing interests.

Additional information
Supplementary information The online version contains supplementary material available at https://doi.org/10.1038/s41545-024-00322-9.

Correspondence and requests for materials should be addressed to Razi Epsztein.